Core-Level X-Ray Spectroscopy of Infinite-Layer Nickelate: LDA + DMFT Study

Keisuke Higashi,[1] Mathias Winder,[2] Jan Kuneš,[2] and Atsushi Hariki[1,*]

[1]Department of Physics and Electronics,
Osaka Prefecture University 1-1 Gakuen-cho, Nakaku, Sakai, Osaka 599-8531, Japan
[2]Institute of Solid State Physics, TU Wien, 1040 Vienna, Austria

(Received 11 May 2021; revised 4 August 2021; accepted 7 September 2021; published 13 October 2021; corrected 11 November 2021 and 23 November 2021)

Motivated by recent core-level x-ray photoemission spectroscopy, x-ray absorption spectroscopy (XAS), and resonant inelastic x-ray scattering (RIXS) experiments for the newly discovered superconducting infinite-layer nickelate, we investigate the core-level spectra of the parent compounds $NdNiO_2$ and $LaNiO_2$ using the combination of local density approximation and dynamical mean-field theory (LDA + DMFT). Adjusting a charge-transfer energy to match the experimental spectra, we determine the optimal model parameters and discuss the nature of the $NdNiO_2$ ground state. We find that self-doping from the Nd $5d$ states in the vicinity of the Fermi energy prohibits opening of a Mott-Hubbard gap in $NdNiO_2$. The present Ni L_3 XAS and RIXS calculation for $LaNiO_2$ cannot explain the difference from $NdNiO_2$ spectra.

DOI: 10.1103/PhysRevX.11.041009

Subject Areas: Computational Physics, Condensed Matter Physics, Strongly Correlated Materials

I. INTRODUCTION

High-T_c superconductivity of cuprates has been a focal point of $3d$ transition-metal oxide (TMO) physics over the past 30 years [1–3]; nevertheless, the underlying mechanism remains elusive. Superconductivity [4] reported recently in layered nickelate $Nd_{0.8}Sr_{0.2}NiO_2$ ($T_c = 9$–15 K) with a similar crystal structure may provide new clues. The fundamental question is whether the electronic structure of $NdNiO_2$ (and $LaNiO_2$) is similar to that of high-T_c cuprates. Naively, one might presume that Ni in the undoped systems is monovalent and, thus, hosts the d^9 ($S = 1/2$) ground state similar to cuprates. However, theoretical studies [5–9] suggest a self-doping from Nd (or La) $5d$ orbitals. Additionally, holes doped to a low-valence Ni^{1+} compound may reside in Ni $3d$ orbitals, unlike in cuprates [2,3,10] or NiO with Ni^{2+} [11], where they occupy the O $2p$ states.

The Ni $2p_{3/2}$ core-level x-ray photoemission spectroscopy (XPS) [12], x-ray absorption spectroscopy (XAS), and resonant inelastic x-ray scattering (RIXS) [9,13] are employed to probe the electronic structure of infinite-layer nickelates. A shoulder observed in the main line of the Ni $2p_{3/2}$ XPS spectra in $NdNiO_2$ [12] is attributed to Ni-Ni charge-transfer (CT) response to the creation of the core hole, a process traditionally called nonlocal screening (NLS) [14]. Generally, NLS provides valuable information about the electronic structure of TMOs [15–18]. For high-T_c cuprates, the NLS in Cu $2p_{3/2}$ XPS is extensively used to determine key parameters, such as the CT energy Δ_{dp}, and more recently to analyze electronic reconstructions due to doping [19–23].

Further information can be obtained with charge-conserving spectroscopies XAS and RIXS. The Ni L_3-edge XAS and RIXS spectra are measured in both $NdNiO_2$ [9,13] and $LaNiO_2$ [9]. Interestingly, a side peak (852.0 eV) is observed in L_3-XAS of $LaNiO_2$, while it is absent in $NdNiO_2$. A low-energy RIXS feature ($E_{\mathrm{loss}} = 0.6$ eV) associated with the XAS side peak is observed in $LaNiO_2$. The difference between the Ni L_3 XAS and RIXS spectra of $NdNiO_2$ and $LaNiO_2$ poses an open question.

In this paper, we use the local-density approximation (LDA) + dynamical mean-filed theory (DMFT) [24–26] to calculate XPS, XAS, and RIXS spectra [16,27–30] of undoped infinite-layer nickelates. By comparison with the available experimental data, we identify the most appropriate CT energy and use it for classification within the Zaanen-Sawatzky-Allen scheme [10].

Material-specific DMFT calculations for $NdNiO_2$ or $LaNiO_2$ were performed by several authors, leading to contradictory conclusions, which can be sorted into two groups: (i) Multiorbital (Hund's metal) physics is crucial [31–34], and (ii) (single-orbital) Mott-Hubbard physics is relevant with little influence of charge-transfer effects or with a small self-doping by Nd $5d$ electrons [35–37]. The

*hariki@pe.osakafu-u.ac.jp

differences, recently addressed by Karp, Hampel, and Millis [38], can be traced to the model parameters, which are not uniquely defined, such as the interaction strength, orbital basis, and, in particular, the double-counting correction. To settle the debate, an experimental input is needed to provide a benchmark for selecting the model parameters.

II. COMPUTATIONAL METHOD

The XPS, XAS, and RIXS simulations start with a standard LDA + DMFT calculation [16,25–28,39]. First, LDA bands for the experimental crystal structure of $NdNiO_2$ and $LaNiO_2$ [4,40] are calculated using the Wien2K package [41,42] and projected onto Wannier basis spanning the Ni $3d$, O $2p$, and Nd (La) $5d$ orbitals [43,44]. The model is augmented with a local electron-electron interaction within the Ni $3d$ shell, parametrized by Coulomb's $U = 5.0$ eV and Hund's $J = 1.0$ eV [31,32,45]. The strong-coupling continuous-time quantum Monte Carlo impurity solver [46–49] is employed with the DMFT cycle to obtain the Ni $3d$ self-energy $\Sigma(i\omega_n)$, which is analytically continued [50] to real frequency after having reached the self-consistency. The calculations are performed at temperature $T = 290$ K.

The XPS, XAS, and RIXS spectra are calculated from the Anderson impurity model augmented with the $2p$ core states and the real-frequency hybridization function discretized into 40–50 levels (per spin and orbital). To this end, we use the configuration-interaction solver; for details, see Refs. [16,29] for XPS and Refs. [27,28,51] for XAS and RIXS simulation.

Determination of Ni $3d$ site energies in the model studied by DMFT involves subtracting the so-called double-counting correction $\mu_{\rm dc}$ from the respective LDA values ($\varepsilon_d^{\rm LDA}$), a procedure accounting for the effect of the dd interaction present in the LDA description. It is clear that $\mu_{\rm dc}$ is of the order of Hartree energy Un_d, but a generally accepted universal expression is not available [26,52,53]. While a similar uncertainty exists also for interaction parameters U and J, impact of their variation on physical properties is usually minor (see Supplemental Material [54] for $NdNiO_2$-specific discussion). Variation of $\mu_{\rm dc}$, on the other hand, may have a profound effect. Therefore, we choose to adjust $\mu_{\rm dc}$ by comparison to the experimental data. Although $\mu_{\rm dc}$ is the parameter entering the calculation, in the discussion we use its linear function $\Delta_{dp} = (\varepsilon_d^{\rm LDA} - \mu_{\rm dc}) + 9U_{dd} - \varepsilon_p^{\rm LDA}$, which sets the scale for the energy necessary to transfer an electron from O $2p$ to Ni $3d$ orbital. Here, $U_{dd} = U - \frac{4}{9}J$ is the average interorbital interaction, and 9 is the Ni $3d$ occupation in the Ni^+ formal valence (similar to the definition of the charge-transfer energy in the cluster model [28,29,55]).

III. ELECTRONIC STRUCTURE

Figure 1 shows the orbitally resolved spectral densities (projected density of states) of $NdNiO_2$ obtained by LDA and LDA + DMFT for $\Delta_{dp} = 4.9$ eV, which we later identify as the optimal parameter choice. Both the LDA and LDA + DMFT yield a metallic state with the Ni $x^2 - y^2$ orbital character dominating around the Fermi level. This general picture is valid in the entire range of studied $\Delta_{dp} = 2.9$–6.9 eV. In Fig. 2, we show the dependence of Ni $x^2 - y^2$ and $3z^2 - r^2$ spectra on Δ_{dp}. Increasing Δ_{dp} corresponds to an upward shift of the bare Ni $3d$ site energies, which is indirectly reflected in the shift of the $3z^2 - r^2$ band. The $x^2 - y^2$ peak at the Fermi level, rather

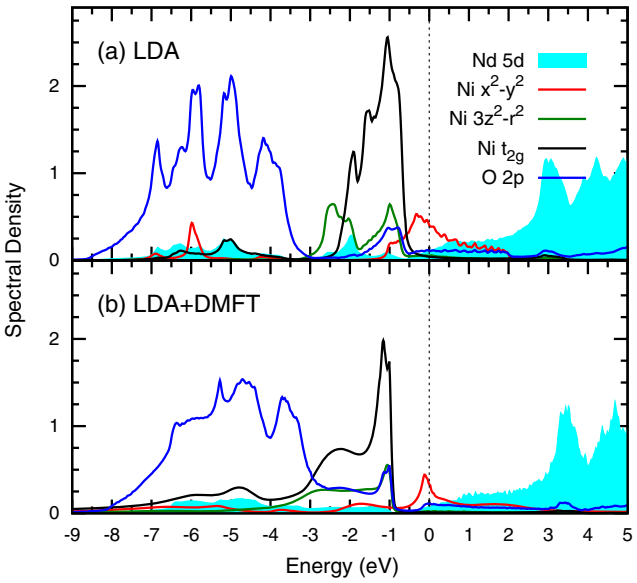

FIG. 1. The one-particle spectral densities of $NdNiO_2$ obtained by (a) LDA and (b) LDA+DMFT (for $\Delta_{dp} = 4.9$ eV).

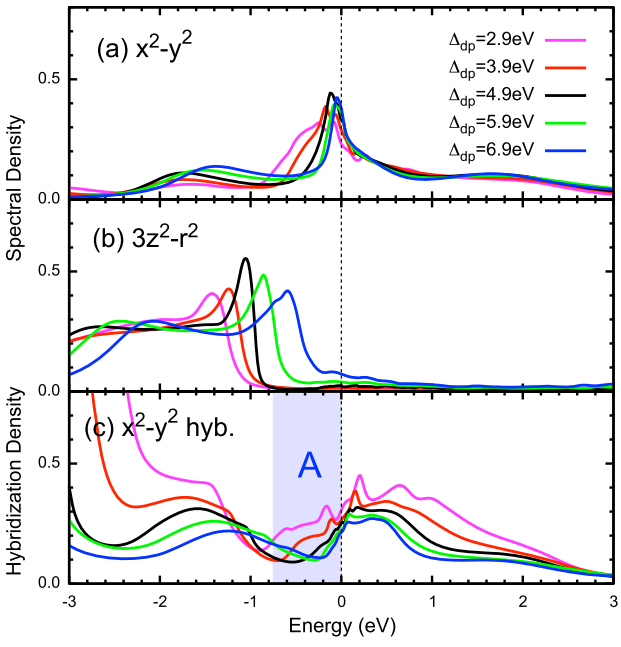

FIG. 2. The DMFT spectral densities for (a) Ni $x^2 - y^2$ and (b) Ni $3z^2 - r^2$ orbitals along with (c) the Ni $x^2 - y^2$ hybridization function computed for different Δ_{dp} values.

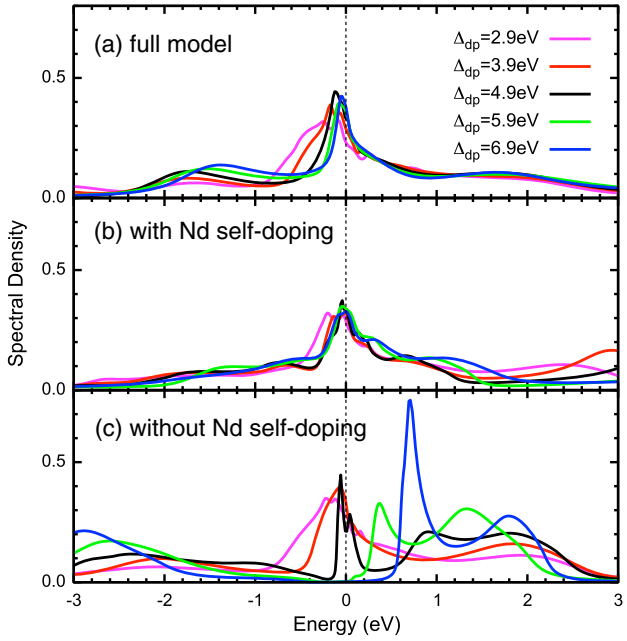

FIG. 3. The $x^2 - y^2$ spectral densities computed in (a) the full model [the same as in Fig. 2(a)], (b) model (i) with a self-doping from Nd d bands, and (c) model (ii) without a self-doping from Nd d bands.

than being shifted, exhibits an increased mass renormalization (reduced width). The amplitude of the $x^2 - y^2$ hybridization function [16,27] around the Fermi level is reduced with increasing Δ_{dp}; in particular, the sizable decrease just below the Fermi level (blue region) has an important implication for the XPS spectra as discussed later. The evolution of $x^2 - y^2$ and $3z^2 - r^2$ occupancies in Fig. 4 shows that, up to $\Delta_{dp} \approx 7$ eV, the $3z^2 - r^2$ is completely filled (the deviation from 2.0 is due to hybridization with empty bands). The physics is, thus, effectively of a single-orbital Hubbard model, and the Ni ion takes a monovalent (Ni^{1+}, d^9) character.

Different from cuprates, the stoichiometric parent compound is metallic. In order to analyze the role of Nd 5d bands, we study two modified models: (i) hybridization between NiO_2 planes and the Nd orbitals is switched off, and (ii) Nd orbitals are removed from the model. In the former case (i) self-doping of the NiO_2 planes from Nd orbitals is possible, while in the latter case (ii) the stoichiometry of the NiO_2 planes cannot change. The evolution of the $x^2 - y^2$ spectral density with Δ_{dp} for (i) and (ii) is shown in Fig. 3. Like the full model, the low-energy spectrum of model (i) remains metallic over the whole studied range of Δ_{dp}. Removing the Nd orbitals (ii) results in progressive mass renormalization with increasing Δ_{dp} and eventually opening of a gap above $\Delta_{dp} = 5.9$ eV. This can be understood as a result of effective weakening of the Ni-O hybridization, i.e., a bandwidth-driven Mott transition. The NiO_2 layers in $NdNiO_2$ can, thus, be viewed as a strongly correlated system in the vicinity of Mott transition, where the insulating state is precluded by the presence of Nd 5d bands [56].

IV. COMPARISON TO EXPERIMENTAL X-RAY SPECTROSCOPIES

A. Ni $2p_{3/2}$ XPS

Next, we investigate the impact of the variation of Δ_{dp} on the core-level spectra. Figure 5 shows the calculated Ni $2p_{3/2}$ XPS spectra of $NdNiO_2$ together with the experimental data [12]. The Ni $2p_{3/2}$ XPS spectrum consists of two components: the main line (852–857 eV) and the CT satellite (861 eV) [16,55]. The core hole created by x rays represents an attractive potential, which induces CT from surrounding atoms to the empty 3d orbital on the excited Ni site. The main line corresponds to the CT screened final states, while the CT satellite corresponds to unscreened ones [14,16,23]. Fu *et al.* [12] observe a shoulder B (approximately 856.5 eV) in the main line. Unlike A, the peak B is absent in the cluster-model spectra [14,29] and, thus, can be ascribed to NLS [12]. The sensitivity of the relative intensity of A and B to Δ_{dp} can be used to locate its value to the interval 4.9–5.9 eV. The observed behavior of the NLS feature B reflects the amplitude of the hybridization function just below the Fermi level [16], the shaded area in Fig. 2(c).

The NLS (B) is known to dominate over the local screening (A) in cuprates, as shown in Fig. 5 for Cu $2p_{3/2}$ XPS in La_2CuO_4 [19]. For small $\Delta_{dp} = 2.9$ eV, a typical value for high-T_c cuprates [10,14,19,23,57], the spectra of $NdNiO_2$ resemble that of La_2CuO_4. Thus, our analysis shows that Δ_{dp} in $NdNiO_2$ is by 2–3 eV larger than in cuprates. The relative size Δ_{dp} and the Hubbard U would place $NdNiO_2$ somewhere between the Mott-Hubbard ($\Delta_{dp} > U$) and CT ($\Delta_{dp} < U$) systems in the Zaanen-Sawatzky-Allen classification of TMOs [10,37,58,59]. The calculated occupations for doped $Nd_{0.775}Sr_{0.225}NiO_2$, shown in Fig. 4 and in

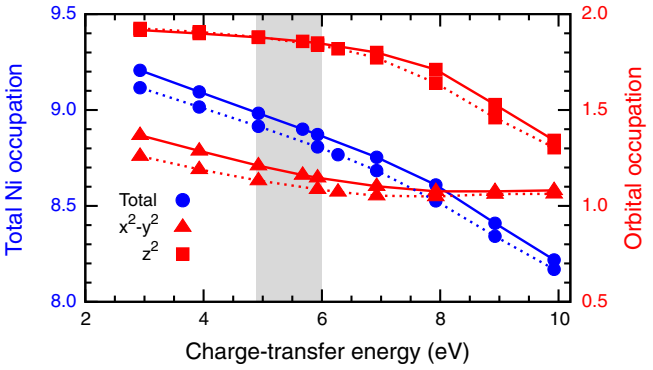

FIG. 4. The DMFT occupation of $x^2 - y^2$ (red, square) and $3z^2 - r^2$ (red, triangle) orbitals and the entire Ni 3d shell (blue, circle) as a function of Δ_{dp}. The full line is obtained for $NdNiO_2$, and the dashed line for $Nd_{0.775}Sr_{0.225}NiO_2$.

Supplemental Material [54], reveal that for optimal Δ_{dp} doped holes are almost equally shared by Ni, Nd, and O sites. This is a remarkable difference to monovalent cuprates or divalent NiO. In these systems of strong charge-transfer character, the doped holes reside predominantly in O $2p$ orbitals, irrespective of a substantial $3d$ spectral weight just below the Fermi level [60]. Moreover, for the optimal Δ_{dp} values inferred above, the doped holes in $NdNiO_2$ do not enter the Ni $3z^2 - r^2$ orbitals (Fig. 4). The single-band Hubbard description is, thus, valid not only for the parent $NdNiO_2$ but also for the superconducting one $Nd_{0.8}Sr_{0.2}NiO_2$, as suggested by Refs. [35–37].

Proximity of NiO_2 layers to a Mott state (precluded by self-doping from Nd) suggests that a superexchange interaction still plays a role despite the metallic state. Using the optimal Δ_{dp}, we arrive [54] at the nearest Ni-Ni antiferromagnetic exchange in the range 40–60 meV. Given the oversimplification of representing spin response of a metal in terms of local moments interactions, this value is consistent with 69 meV inferred from the RIXS experiment on a related compound $La_4Ni_3O_8$ [61].

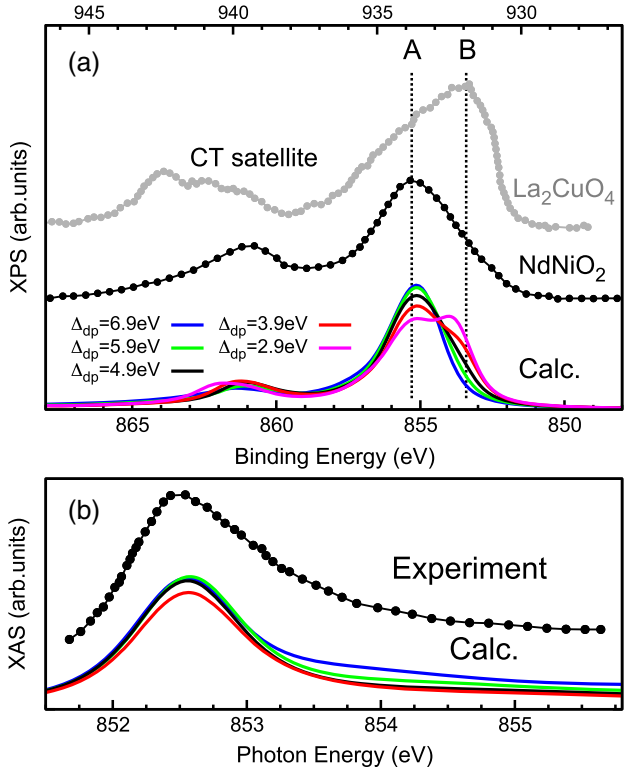

FIG. 5. (a) Ni $2p_{3/2}$ XPS spectra and (b) Ni $2p_{3/2}$ XAS spectra of $NdNiO_2$ calculated by the LDA + DMFT method for different Δ_{dp} values. The experimental data [9,12] are shown together. For comparison, experimental Cu $2p_{3/2}$ XPS data of La_2CuO_4 are shown (gray) [19]. The spectral broadening is taken into account using a Lorentzian 300 meV (HWHM) and a Gaussian 250 meV (HWHM) for XAS and a Lorentzian 500 meV and a Gaussian 400 meV for XPS. The XPS spectra with different broadening widths can be found in Supplemental Material [54].

The calculated $LaNiO_2$ spectra in Fig. 6(a) show similar behavior to $NdNiO_2$.

B. Ni $2p_{3/2}$ XAS and RIXS

As expected for Ni^{1+} systems with a d^9 configuration, the experimental Ni $2p_{3/2}$ XAS of $NdNiO_2$ shows a sharp peak corresponding to the electron excitation from the $2p_{3/2}$ to an empty $x^2 - y^2$ orbital [Fig. 5(b)]. The XAS main peak is accompanied by a broad tail attributed to the hybridization with metallic bands. The theoretical results in Fig. 5(b) reproduce the experimental data reasonably well; however, the weak dependence on Δ_{dp} does not allow one to draw conclusions about its value.

The RIXS spectra, on the other hand, exhibit fine changes with the Δ_{dp} values; see Fig. 7. The spectra at all Δ_{dp} values contain a strong Raman-like (RL) feature (at constant $E_{\rm loss}$ irrespective of the incident photon energies $E_{\rm in}$) at $E_{\rm loss} \sim 1$ eV and a fluorescencelike (FL) feature ($E_{\rm loss}$ linearly increases with $E_{\rm in}$). The RL feature arises from $t_{2g} \rightarrow x^2 - y^2$ excitation, and its width (in $E_{\rm loss}$) reflects a rapid decay of this local "exciton." With increasing Δ_{dp}, the RL feature shifts to lower energies, due to the upward shift to the t_{2g} bands [similar to $3z^2 - r^2$ shown in Fig. 2(b)], while the $x^2 - y^2$ peaks remain pinned in the vicinity of the Fermi level. The main variation of the RIXS spectra with increasing Δ_{dp} concerns the behavior of the FL part, the onset of which is pushed to higher $E_{\rm loss}$. For

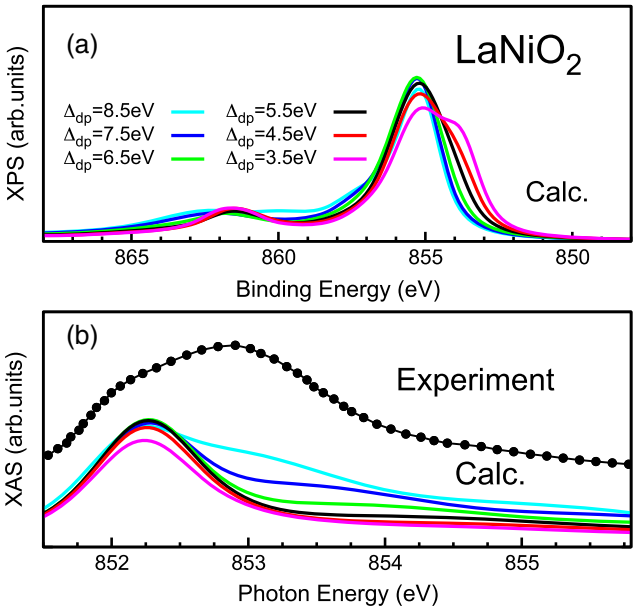

FIG. 6. (a) Ni $2p_{3/2}$ XPS spectra and (b) Ni $2p_{3/2}$ XAS spectra of $LaNiO_2$ calculated by the LDA + DMFT method for different Δ_{dp} values. The spectral broadening is taken into account using a Lorentzian 300 meV (HWHM) and a Gaussian 250 meV (HWHM) for XAS and a Lorentzian 500 meV and a Gaussian 400 meV for XPS.

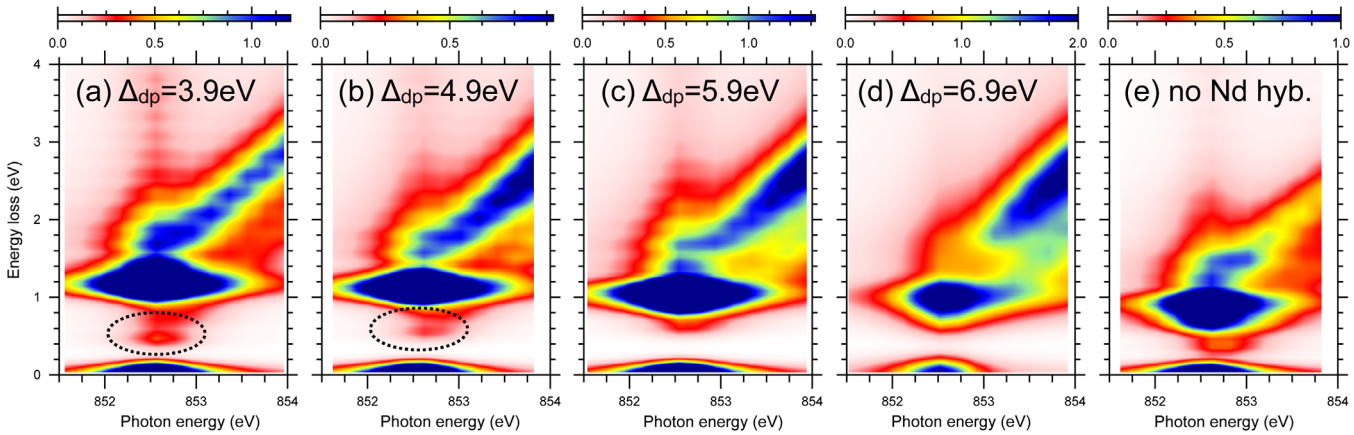

FIG. 7. The Ni L_3 RIXS spectra of $NdNiO_2$ calculated for (a) $\Delta_{dp} = 3.9$ eV, (b) $\Delta_{dp} = 4.9$ eV, (c) $\Delta_{dp} = 5.9$ eV, and (d) $\Delta_{dp} = 6.9$ eV. (e) The Ni L_3 RIXS spectra calculated for the model without the hybridization between Nd $5d$ and the NiO_2 plane ($\Delta_{dp} = 4.9$ eV). The spectral broadening is considered using a Gaussian of 100 meV (HWHM).

$\Delta_{dp} = 4.9$ eV, deduced from the XPS data, the FL feature sets in below the RL feature at around $E_{\text{loss}} \sim 0.6$ eV. The coexisting RL and FL features above well capture the experimental data by Hepting *et al.* [9] and Rossi *et al.* [13]. Artificial suppression of hybridization to Nd $5d$ states [Fig. 7(e)] leads to a reduced intensity of the FL feature and only a moderate modification of the low-energy spectra supporting the conclusion about the electron-reservoir role of Nd $5d$ states.

Finally, we discuss XAS and RIXS spectra in $LaNiO_2$ (the experimental XPS data are not available at the moment). The experimental XAS spectra of $LaNiO_2$ [9] are clearly distinct from $NdNiO_2$. A side peak at 852.0 eV is attributed to Ni-La hybridization effect by Hepting *et al.* [9] based on a simplified impurity model simulation. The LDA + DMFT calculations (including Ni-La hybridization) do not support this conclusion, as they do not match the experimental XAS spectra. While large Δ_{dp} gives rise to a high-energy XAS shoulder (Fig. 6), it does not improve the agreement of the RIXS spectra, shown in Fig. 8. We have to conclude that the present LDA + DMFT description of $LaNiO_2$ does not match the experiment for any choice of Δ_{dp}.

We propose that the problem lies on the experimental side; i.e., the measured spectra do not represent a perfect $LaNiO_2$ crystal. We argue by the success of the present method for a broad spectrum of transition-metal oxides [16] including $NdNiO_2$ as well as the absence of an obvious source of difference between $NdNiO_2$ and $LaNiO_2$. On the experimental side, we point out recent studies [62,63] reporting superconductivity in Sr-doped $LaNiO_2$, suggesting that $NdNiO_2$ and $LaNiO_2$ are not that different after all. Spectroscopic experiments on these new $LaNiO_2$ samples are needed to resolve the present discrepancy.

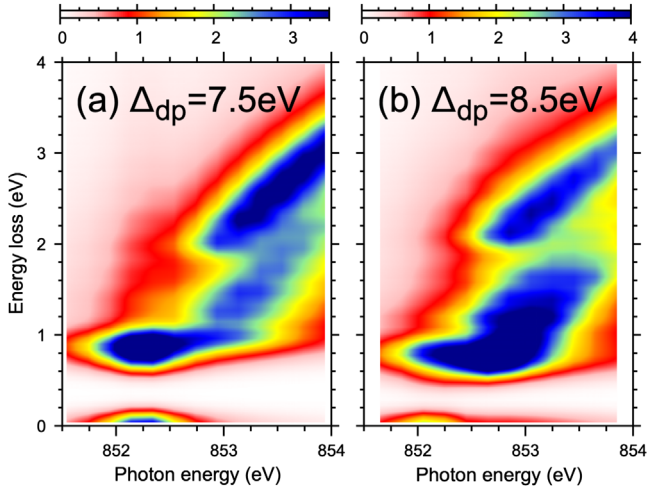

FIG. 8. The Ni L_3 RIXS spectra of $LaNiO_2$ calculated for (a) $\Delta_{dp} = 7.5$ eV and (b) $\Delta_{dp} = 8.5$ eV. The spectral broadening is considered using a Gaussian of 100 meV (HWHM).

V. CONCLUSIONS

We have presented a comprehensive analysis of Ni $2p_{3/2}$ core-level XPS, XAS, and RIXS in infinite-layer nickelates ($NdNiO_2$ and $LaNiO_2$) with the LDA + DMFT approach. Comparison to the experimental spectra allowed us to determine the CT parameter (double-counting correction) and make the following conclusions about the electronic structure. Undoped $NdNiO_2$ is nearly monovalent (Ni^{1+}, d^9) with a small self-doping from the Nd $5d$ band. Only the Ni $x^2 - y^2$ orbitals are partially filled, and multiorbital physics does not play an important role for the stoichiometric as well as slightly hole-doped compound. Unlike in cuprates, the Ni-O hybridization does not play an important role in connection with doping—doped holes reside predominantly on the Ni sites. The physics of $NdNiO_2$ described effectively by a single-band Hubbard model [35–37] is consistent with the available core-level spectroscopies. While the present calculations provide a

good description of the experimental core-level spectra of $NdNiO_2$, we cannot explain the qualitative difference between the reported $NdNiO_2$ and $LaNiO_2$ XAS and RIXS spectra.

ACKNOWLEDGMENTS

We thank M. Kitatani, K. Yamagami, T. Uozumi, H. Ikeno, L. Si, M.-J. Huang, and R.-P. Wang for valued discussions. A. H., M. W., and J. K. were supported by the European Research Council (ERC) under the European Union's Horizon 2020 research and innovation program (Grant Agreement No. 646807-EXMAG). A. H. was supported by JSPS KAKENHI Grant No. 21K13884. The numerical calculations were performed at the Vienna Scientific Cluster (VSC).

[1] J. G. Bednorz and K. A. Müller, *Possible High* T_c *Superconductivity in the Ba-La-Cu-O System*, Z. Phys. B **64**, 189 (1986).

[2] M. Imada, A. Fujimori, and Y. Tokura, *Metal-Insulator Transitions*, Rev. Mod. Phys. **70**, 1039 (1998).

[3] E. Dagotto, *Correlated Electrons in High-Temperature Superconductors*, Rev. Mod. Phys. **66**, 763 (1994).

[4] D. Li, K. Lee, B. Y. Wang, M. Osada, S. Crossley, H. R. Lee, Y. Cui, Y. Hikita, and H. Y. Hwang, *Superconductivity in an Infinite-Layer Nickelate*, Nature (London) **572**, 624 (2019).

[5] A. S. Botana and M. R. Norman, *Similarities and Differences between* $LaNiO_2$ *and* $CaCuO_2$ *and Implications for Superconductivity*, Phys. Rev. X **10**, 011024 (2020).

[6] J. Krishna, H. LaBollita, A. O. Fumega, V. Pardo, and A. S. Botana, *Effects of Sr Doping on the Electronic and Spin-State Properties of Infinite-Layer Nickelates: Nature of Holes*, Phys. Rev. B **102**, 224506 (2020).

[7] K.-W. Lee and W. E. Pickett, *Infinite-Layer* $LaNio_2$*:* Ni^{1+} *Is Not* Cu^{2+}, Phys. Rev. B **70**, 165109 (2004).

[8] G.-M. Zhang, Y.-F. Yang, and F.-C. Zhang, *Self-Doped Mott Insulator for Parent Compounds of Nickelate Superconductors*, Phys. Rev. B **101**, 020501(R) (2020).

[9] M. Hepting *et al.*, *Electronic Structure of the Parent Compound of Superconducting Infinite-Layer Nickelates*, Nat. Mater. **19**, 381 (2020).

[10] J. Zaanen, G. A. Sawatzky, and J. W. Allen, *Band Gaps and Electronic Structure of Transition-Metal Compounds*, Phys. Rev. Lett. **55**, 418 (1985).

[11] J. Kuneš, V. I. Anisimov, S. L. Skornyakov, A. V. Lukoyanov, and D. Vollhardt, *NiO: Correlated Band Structure of a Charge-Transfer Insulator*, Phys. Rev. Lett. **99**, 156404 (2007).

[12] Y. Fu, L. Wang, H. Cheng, S. Pei, X. Zhou, J. Chen, S. Wang, R. Zhao, W. Jiang, C. Liu, M. Huang, X. W. Wang, Y. Zhao, D. Yu, F. Ye, S. Wang, and J.-W. Mei, *Electronic Structures and Spin Fluctuations in Nickelate Oxide* $NdNiO_2$, arXiv:1911.03177.

[13] M. Rossi, H. Lu, A. Nag, D. Li, M. Osada, K. Lee, B. Y. Wang, S. Agrestini, M. Garcia-Fernandez, Y. D. Chuang, Z. X. Shen, H. Y. Hwang, B. Moritz, Ke-Jin Zhou, T. P. Devereaux, and W. S. Lee, *Orbital and Spin Character of Doped Carriers in Infinite-Layer Nickelates*, arXiv:2011.00595.

[14] M. A. van Veenendaal and G. A. Sawatzky, *Nonlocal Screening Effects in 2p X-Ray Photoemission Spectroscopy Core-Level Line Shapes of Transition Metal Compounds*, Phys. Rev. Lett. **70**, 2459 (1993).

[15] M. van Veenendaal, *Competition between Screening Channels in Core-Level X-Ray Photoemission as a Probe of Changes in the Ground-State Properties of Transition-Metal Compounds*, Phys. Rev. B **74**, 085118 (2006).

[16] A. Hariki, T. Uozumi, and J. Kuneš, *LDA+DMFT Approach to Core-Level Spectroscopy: Application to 3d Transition Metal Compounds*, Phys. Rev. B **96**, 045111 (2017).

[17] M. Taguchi and G. Panaccione, in *Hard X-Ray Photoelectron Spectroscopy (HAXPES)*, edited by J. C. Woicik (Springer International, Cham, 2016), pp. 197–216.

[18] M. Taguchi, M. Matsunami, Y. Ishida, R. Eguchi, A. Chainani, Y. Takata, M. Yabashi, K. Tamasaku, Y. Nishino, T. Ishikawa, Y. Senba, H. Ohashi, and S. Shin, *Revisiting the Valence-Band and Core-Level Photoemission Spectra of NiO*, Phys. Rev. Lett. **100**, 206401 (2008).

[19] M. Taguchi, A. Chainani, K. Horiba, Y. Takata, M. Yabashi, K. Tamasaku, Y. Nishino, D. Miwa, T. Ishikawa, T. Takeuchi, K. Yamamoto, M. Matsunami, S. Shin, T. Yokoya, E. Ikenaga, K. Kobayashi, T. Mochiku, K. Hirata, J. Hori, K. Ishii, F. Nakamura, and T. Suzuki, *Evidence for Suppressed Screening on the Surface of High Temperature* $La_{2-x}Sr_xCuO_4$ *and* $Nd_{2-x}Ce_xCuO_4$ *Superconductors*, Phys. Rev. Lett. **95**, 177002 (2005).

[20] M. Horio, Y. Krockenberger, K. Yamamoto, Y. Yokoyama, K. Takubo, Y. Hirata, S. Sakamoto, K. Koshiishi, A. Yasui, E. Ikenaga, S. Shin, H. Yamamoto, H. Wadati, and A. Fujimori, *Electronic Structure of Ce-Doped and -Undoped* Nd_2CuO_4 *Superconducting Thin Films Studied by Hard X-Ray Photoemission and Soft X-Ray Absorption Spectroscopy*, Phys. Rev. Lett. **120**, 257001 (2018).

[21] K. Okada and A. Kotani, *Nonlocal Screening Effects on Core-Level Photoemission Spectra Investigated by Large-Cluster Models*, Phys. Rev. B **52**, 4794 (1995).

[22] M. A. van Veenendaal, G. A. Sawatzky, and W. A. Groen, *Electronic Structure of* $Bi_2Sr_2Ca_{1-x}Y_xCu_2O_{8+\delta}$*: Cu 2p X-Ray-Photoelectron Spectra and Occupied and Unoccupied Low-Energy States*, Phys. Rev. B **49**, 1407 (1994).

[23] M. Taguchi, A. Chainani, N. Kamakura, K. Horiba, Y. Takata, M. Yabashi, K. Tamasaku, Y. Nishino, D. Miwa, T. Ishikawa, S. Shin, E. Ikenaga, T. Yokoya, K. Kobayashi, T. Mochiku, K. Hirata, and K. Motoya, *Bulk Screening in Core-Level Photoemission from Mott-Hubbard and Charge-Transfer Systems*, Phys. Rev. B **71**, 155102 (2005).

[24] W. Metzner and D. Vollhardt, *Correlated Lattice Fermions in* $d = \infty$ *Dimensions*, Phys. Rev. Lett. **62**, 324 (1989).

[25] A. Georges, G. Kotliar, W. Krauth, and M. J. Rozenberg, *Dynamical Mean-Field Theory of Strongly Correlated Fermion Systems and the Limit of Infinite Dimensions*, Rev. Mod. Phys. **68**, 13 (1996).

[26] G. Kotliar, S. Y. Savrasov, K. Haule, V. S. Oudovenko, O. Parcollet, and C. A. Marianetti, *Electronic Structure Calculations with Dynamical Mean-Field Theory*, Rev. Mod. Phys. **78**, 865 (2006).

[27] A. Hariki, M. Winder, and J. Kuneš, *Continuum Charge Excitations in High-Valence Transition-Metal Oxides Revealed by Resonant Inelastic X-Ray Scattering*, Phys. Rev. Lett. **121**, 126403 (2018).

[28] A. Hariki, M. Winder, T. Uozumi, and J. Kuneš, LDA + DMFT *Approach to Resonant Inelastic X-Ray Scattering in Correlated Materials*, Phys. Rev. B **101**, 115130 (2020).

[29] M. Ghiasi, A. Hariki, M. Winder, J. Kuneš, A. Regoutz, T.-L. Lee, Y. Hu, J.-P. Rueff, and F. M. F. de Groot, *Charge-Transfer Effect in Hard X-Ray* 1*s and* 2*p Photoemission Spectra:* LDA + DMFT *and Cluster-Model Analysis*, Phys. Rev. B **100**, 075146 (2019).

[30] J. Kolorenč, *Theory of Resonant X-Ray Emission Spectra in Compounds with Localized f Electrons*, Physica (Amsterdam) **536B**, 695 (2018).

[31] Y. Wang, C.-J. Kang, H. Miao, and G. Kotliar, *Hund's Metal Physics: From* $SrNiO_2$ *to* $LaNiO_2$, Phys. Rev. B **102**, 161118(R) (2020).

[32] C.-J. Kang and G. Kotliar, *Optical Properties of the Infinite-Layer* $La_{1-x}Sr_xNiO_2$ *and Hidden Hund's Physics*, Phys. Rev. Lett. **126**, 127401 (2021).

[33] F. Petocchi, V. Christiansson, F. Nilsson, F. Aryasetiawan, and P. Werner, *Normal State of* $Nd_{1-x}Sr_xNiO_2$ *from Self-Consistent gw* + EDMFT, Phys. Rev. X **10**, 041047 (2020).

[34] F. Lechermann, *Multiorbital Processes Rule the* $Nd_{1-x}Sr_xNiO_2$ *Normal State*, Phys. Rev. X **10**, 041002 (2020).

[35] J. Karp, A. S. Botana, M. R. Norman, H. Park, M. Zingl, and A. Millis, *Many-Body Electronic Structure of* $NdNiO_2$ *and* $CaCuO_2$, Phys. Rev. X **10**, 021061 (2020).

[36] M. Kitatani, L. Si, O. Janson, R. Arita, Z. Zhong, and K. Held, *Nickelate Superconductors—A Renaissance of the One-Band Hubbard Model*, npj Quantum Mater. **5**, 59 (2020).

[37] J. Karp, A. Hampel, M. Zingl, A. S. Botana, H. Park, M. R. Norman, and A. J. Millis, *Comparative Many-Body Study of* $Pr_4Ni_3O_8$ *and* $NdNiO_2$, Phys. Rev. B **102**, 245130 (2020).

[38] J. Karp, A. Hampel, and A. J. Millis, *Dependence of* DFT + DMFT *Results on the Construction of the Correlated Orbitals*, Phys. Rev. B **103**, 195101 (2021).

[39] J. Kuneš, I. Leonov, M. Kollar, K. Byczuk, V. I. Anisimov, and D. Vollhardt, *Dynamical Mean-Field Approach to Materials with Strong Electronic Correlations*, Eur. Phys. J. Special Topics **180**, 5 (2009).

[40] M. A. Hayward, M. A. Green, M. J. Rosseinsky, and J. Sloan, *Sodium Hydride as a Powerful Reducing Agent for Topotactic Oxide Deintercalation: Synthesis and Characterization of the Nickel (i) Oxide LaNiO2*, J. Am. Chem. Soc. **121**, 8843 (1999).

[41] P. Blaha, K. Schwarz, G. Madsen, D. Kvasnicka, and J. Luitz, *Wien2K, An Augmented Plane Wave+Local Orbitals Program for Calculating Crystal Properties* (Karlheinz Schwarz, Technische Universitat Wien, Austria, 2001), ISBN 3-9501031-1-2.

[42] The Nd 4*f* states in $NdNiO_2$ are treated as partially filled core states.

[43] J. Kuneš, R. Arita, P. Wissgott, A. Toschi, H. Ikeda, and K. Held, *Wien2Wannier: From Linearized Augmented Plane Waves to Maximally Localized Wannier Functions*, Comput. Phys. Commun. **181**, 1888 (2010).

[44] A. A. Mostofi, J. R. Yates, G. Pizzi, Y.-S. Lee, I. Souza, D. Vanderbilt, and N. Marzari, *An Updated Version of Wannier90: A Tool for Obtaining Maximally-Localised Wannier Functions*, Comput. Phys. Commun. **185**, 2309 (2014).

[45] S. Ryee, H. Yoon, T. J. Kim, M. Y. Jeong, and M. J. Han, *Induced Magnetic Two-Dimensionality by Hole Doping in the Superconducting Infinite-Layer Nickelate* $Nd_{1-x}Sr_xNiO_2$, Phys. Rev. B **101**, 064513 (2020).

[46] P. Werner, A. Comanac, L. de' Medici, M. Troyer, and A. J. Millis, *Continuous-Time Solver for Quantum Impurity Models*, Phys. Rev. Lett. **97**, 076405 (2006).

[47] L. Boehnke, H. Hafermann, M. Ferrero, F. Lechermann, and O. Parcollet, *Orthogonal Polynomial Representation of Imaginary-Time Green's Functions*, Phys. Rev. B **84**, 075145 (2011).

[48] H. Hafermann, K. R. Patton, and P. Werner, *Improved Estimators for the Self-Energy and Vertex Function in Hybridization-Expansion Continuous-Time Quantum Monte Carlo Simulations*, Phys. Rev. B **85**, 205106 (2012).

[49] A. Hariki, A. Yamanaka, and T. Uozumi, *Theory of Spin-State Selective Nonlocal Screening in Co 2p X-Ray Photoemission Spectrum of LaCoO3*, J. Phys. Soc. Jpn. **84**, 073706 (2015).

[50] M. Jarrell and J. E. Gubernatis, *Bayesian Inference and the Analytic Continuation of Imaginary-Time Quantum Monte Carlo Data*, Phys. Rep. **269**, 133 (1996).

[51] M. Winder, A. Hariki, and J. Kuneš, *X-Ray Spectroscopy of the Rare-Earth Nickelate* $LuNiO_3$*:* LDA + DMFT *Study*, Phys. Rev. B **102**, 085155 (2020).

[52] M. Karolak, G. Ulm, T. Wehling, V. Mazurenko, A. Poteryaev, and A. Lichtenstein, *Double Counting in* {LDA} + DMFT *the Example of NiO*, J. Electron Spectrosc. Relat. Phenom. **181**, 11 (2010).

[53] K. Haule, *Exact Double Counting in Combining the Dynamical Mean Field Theory and the Density Functional Theory*, Phys. Rev. Lett. **115**, 196403 (2015).

[54] See Supplemental Material at http://link.aps.org/supplemental/10.1103/PhysRevX.11.041009 for model-parameter dependence of Ni density of states, hybridization intensity, and Ni 2*p* XPS spectra.

[55] F. de Groot and A. Kotani, *Core Level Spectroscopy of Solids* (CRC, Boca Raton, FL, 2014).

[56] M. Hirayama, T. Tadano, Y. Nomura, and R. Arita, *Materials Design of Dynamically Stable* d^9 *Layered Nickelates*, Phys. Rev. B **101**, 075107 (2020).

[57] J. Ghijsen, L. H. Tjeng, J. van Elp, H. Eskes, J. Westerink, G. A. Sawatzky, and M. T. Czyzyk, *Electronic Structure of* Cu_2O *and CuO*, Phys. Rev. B **38**, 11322 (1988).

[58] Y. Nomura, T. Nomoto, M. Hirayama, and R. Arita, *Magnetic Exchange Coupling in Cuprate-Analog* d^9 *Nickelates*, Phys. Rev. Research **2**, 043144 (2020).

[59] Y. Nomura, M. Hirayama, T. Tadano, Y. Yoshimoto, K. Nakamura, and R. Arita, *Formation of a Two-Dimensional Single-Component Correlated Electron System and Band Engineering in the Nickelate Superconductor* $NdNiO_2$, Phys. Rev. B **100**, 205138 (2019).

[60] J. Kuneš, V. I. Anisimov, A. V. Lukoyanov, and D. Vollhardt, *Local Correlations and Hole Doping in NiO: A Dynamical Mean-Field Study*, Phys. Rev. B **75**, 165115 (2007).

[61] J. Q. Lin, P. V. Arribi, G. Fabbris, A. S. Botana, D. Meyers, H. Miao, Y. Shen, D. G. Mazzone, J. Feng, S. G. Chiuzbáian, A. Nag, A. C. Walters, M. García-Fernández, K.-J. Zhou, J. Pelliciari, I. Jarrige, J. W. Freeland, J. Zhang, J. F. Mitchell, V. Bisogni, X. Liu, M. R. Norman, and M. P. M. Dean, *Strong Superexchange in a $d^{9-\delta}$ Nickelate Revealed by Resonant Inelastic X-Ray Scattering*, Phys. Rev. Lett. **126**, 087001 (2021).

[62] S. W. Zeng, C. J. Li, L. E. Chow, Y. Cao, Z. T. Zhang, C. S. Tang, X. M. Yin, Z. S. Lim, J. X. Hu, P. Yang, and A. Ariando, *Superconductivity in Infinite-Layer Lanthanide Nickelates*, arXiv:2105.13492.

[63] M. Osada, B. Y. Wang, B. H. Goodge, S. P. Harvey, K. Lee, D. Li, L. F. Kourkoutis, and H. Y. Hwang, *Nickelate Superconductivity without Rare-Earth Magnetism:* $(La, sr)NiO_2$, arXiv:2105.13494.

Correction: The captions to Figs. 6 and 7 were inadvertently switched during the production cycle and have been set right.

Second Correction: The text citations to Figs. 6 and 7 in Sec. IV B were inadvertently switched and have been remedied.